

Prediction of global patterns of dominant quasi-biweekly oscillation by the NCEP Climate Forecast System version 2

Xiaolong Jia · Song Yang · Xun Li ·
Yunyun Liu · Hui Wang · Xiangwen Liu ·
Scott Weaver

Received: 27 December 2012 / Accepted: 8 July 2013 / Published online: 25 July 2013
© Springer-Verlag Berlin Heidelberg 2013

Abstract Daily output from the hindcasts by the National Centers for Environmental Prediction (NCEP) Climate Forecast System version 2 (CFSv2) is analyzed to understand the skill of forecasting atmospheric variability on quasi-biweekly (QBW) time scale. Eight dominant quasi-biweekly oscillation (QBWO) modes identified by the extended empirical orthogonal function analysis are focused. In the CFSv2, QBW variability exhibits a significant weakening tendency with lead time for all seasons. For most QBWO modes, the variance drops to only 50 % of the initial value at lead time of 11–15 days. QBW variability has better prediction skill in the winter hemisphere than in the summer hemisphere. Skillful forecast can reach about 10–15 days for most modes but those in the winter

hemisphere have better forecast skills. Among the eight QBWO modes, the North Pacific mode and the South Pacific (SP) mode have the highest forecast skills while the Asia–Pacific mode and the Central American mode have the lowest skills. For the Asia–Pacific and Central American modes, the forecasted QBWO phase shows an obvious eastward shift with increase in lead time compared to observations, indicating a smaller propagating speed. However, the predicted feature for the SP mode is more realistic. Air–sea coupling on the QBW time scale is perhaps responsible for the different prediction skills for different QBWO modes. In addition, most QBWO modes have better forecasting skills in El Niño years than in La Niña years. Different dynamical mechanisms for various QBWO modes may be partially responsible for the differences in prediction skill among different QBWO modes.

This paper is a contribution to the Topical Collection on Climate Forecast System Version 2 (CFSv2). CFSv2 is a coupled global climate model and was implemented by National Centers for Environmental Prediction (NCEP) in seasonal forecasting operations in March 2011. This Topical Collection is coordinated by Jin Huang, Arun Kumar, Jim Kinter and Annarita Mariotti.

X. Jia · Y. Liu · X. Liu
National Climate Center, China Meteorological Administration,
Beijing, China

S. Yang (✉)
School of Environmental Science and Engineering,
Sun Yat-sen University, 135 West Xingang Road,
Guangzhou 510275, Guangdong, China
e-mail: yangsong3@mail.sysu.edu.cn

X. Li
Hainan Meteorological Service, China Meteorological
Administration, Haikou, Hainan, China

H. Wang · S. Weaver
NOAA Climate Prediction Center, College Park, MD, USA

Keywords Quasi-biweekly oscillation ·
Prediction skill · Monsoons · ENSO

1 Introduction

Intra-seasonal oscillation is one of the most important components of the tropical atmospheric variations that significantly affect the local weather and climate as well as the global atmospheric circulation. It generally involves two major modes: the Madden Julian Oscillation (MJO) with a characteristic period of 30–60 days (Madden and Julian 1971, 1972) and the quasi-biweekly oscillation (QBWO) with a typical time band of 10–20 days (e.g. Krishnamurti and Ardanuy 1980; Chen and Chen 1993, 1995; Fukutomi and Yasunari 1999, 2002; Wen and Zhang 2007; Jiang and Lau 2008; Kikuchi and Wang 2009; Wen et al. 2011; Jia and Yang 2013). Previous studies have

indicated that both the QBWO and MJO influence the active and break phases of the Indian summer monsoon (e.g. Krishnamurti and Ardanuy 1980; Yasunari 1981; Chen and Chen 1993, 1995; Goswami et al. 2003) and the South China Sea (SCS) monsoon (e.g. Chen et al. 2000; Mao and Chan 2005; Zhou and Chan 2005; Lin and Li 2008). The QBWO also plays an important role in the interaction between the summer monsoons in East Asia and the SCS (Chen et al. 2000). The East Asian subtropical monsoon, represented by the Mei-yu and Baiu fronts, is significantly influenced by the transition of QBWO (e.g. Yang et al. 2010; Jia and Yang 2013). In addition, the North Pacific tropical cyclone activity is also modulated by QBWO (Li et al. 2012). The QBWO associated with the North American monsoon is also investigated by many studies (e.g. Mullen et al. 1998; Kiladis and Hall-McKim 2004; Jiang and Waliser 2009; Wen et al. 2011). QBWO is a predominant component not only in the Asian and North American monsoon regions but also in other subtropical regions. Kikuchi and Wang (2009) defined eight QBWO modes in a global perspective, including three boreal summer modes in Asia–Pacific, Central America, and subtropical South Pacific (SP) and five austral summer modes in the Australia–southwest Pacific, South Africa–Indian Ocean, South America–Atlantic, subtropical North Pacific, and North Atlantic–North Africa.

At present, dynamical prediction of the MJO has been a popular subject (e.g. Vitart et al. 2007; Lin et al. 2008; Agudelo et al. 2009; Seo 2009; Gottschalck et al. 2010; Rashid et al. 2011) and a skillful forecast can reach 21 days (Rashid et al. 2011). However, few attempts have been made to dynamically predict QBWO. In this paper, we examine the skill of forecasting global dominant QBWO modes by the National Centers for Environmental Prediction (NCEP) Climate Forecast System (CFS) version 2 (CFSv2; Saha et al. 2013). The CFSv2 is a fully coupled atmosphere–ocean–land–sea ice dynamical seasonal prediction system, which replaced the CFS version 1 (Saha et al. 2006) for operations at the NCEP in March 2011. The CFSv2 has upgrades to nearly all aspects of the data assimilation and forecast model components of the system, and greatly improves the forecast skills in many aspects over the CFSv1, such as the MJO, 2-m temperatures over the US, and global SST (Saha et al. 2013).

In Sect. 2, model output, observational data, and analysis methods are briefly described. A general examination of the prediction of quasi-biweekly variability by the CFSv2 is shown in Sect. 3. Skills of prediction of the eight global dominant QBWO modes defined by the extended empirical orthogonal function (EEOF) are analyzed in Sect. 4. A discussion and summary are given in Sects. 5 and 6, respectively.

2 Model output, observational data and analysis methods

The retrospective forecast data are from the 45-day hindcasts run by the CFSv2 initiated from every 0, 6, 12, and 18 UTC cycle over the 12-year period from 1999 to 2010. Daily mean outputs, including outgoing longwave radiation (OLR), precipitation, surface temperature, and 850-hPa winds, are analyzed.

The observations used for model verification include the daily OLR dataset from the National Oceanic and Atmospheric Administration (NOAA) advanced very high resolution radiometer (AVHRR; Liebmann and Smith 1996), and daily OLR, circulation variables, surface temperature and precipitation from the NCEP CFS Reanalysis (CFSR; Saha et al. 2010). The CFSR is a coupled atmosphere–ocean–land–sea ice reanalysis product and provides reliable estimates of the atmospheric and oceanic state (Xue et al. 2010; Wang et al. 2010).

Using a tracking method and the EEOF analysis, Kikuchi and Wang (2009) defined eight QBWO modes in a global perspective. These modes include three boreal summer patterns in Asia–Pacific (AM mode), Central America (CA mode), and subtropical SP mode and five austral summer patterns in the Australia–Southwest Pacific (AU–SP mode), South Africa–Indian Ocean (SAF mode), South America–Atlantic (SAM mode), subtropical North Pacific (NP mode), and North Atlantic–North Africa regions (NAF mode). In this study, the Lanczos filter (Duchon 1979) is used to obtain the 10–20-day band-pass filtered time series representing the QBWO variability. Considering that the response of the filter is different for different data window lengths, data processing methods are completely the same for both forecasts and observations when applying the 10–20-day band-pass filtering. For observations, the length of data is 92 days (90 days) for JJA (DJF), and then a 10–20-day band pass filtering can be applied in these data. The CFSv2 hindcasts were made for the period from 1999 to 2010 initiated from 0, 6, 12, and 18UTC every day. All hindcasts were run for 45 days and daily mean output data are used. Therefore, we have a total of 4,380 (365 days \times 12 years) forecasts and each forecast produces 45-day results. Thus, for each lead time (total available lead time is 45 days from 1 to 45 days), we have 4,380 forecast results, which can form a consecutive time series at each lead time. For example, the output of first day for all 4,380 forecasts can form a forecast series from 1 January 1999 to 31 December 2010, which represents the forecast for the lead time of 1 day. The output of the second day can construct a series from 2 January 1999 to 1 January 2011, which represents the forecast for the lead time of 2 days. The last day's output forms a series that is from 14 February 1999 to 13 February 2011, representing

the forecast for 45-day lead. Consequently, we can extract the data of 92 day for JJA (total 12 years) and the data of 90 days for DJF (totally 11 years) from these 4,380 forecast results for each lead time. Then we can apply the 10–20-day band-pass filtering on these data of 92 days and 90 days in forecast just the same as applied on observations.

Following Kikuchi and Wang (2009), eight global QBWO modes are extracted by using an EEOF analysis, which is capable of describing a sequence of convective disturbances in an efficient way (Weare and Nasstrom 1982). Considering that 7 days are roughly the half periodicity of QBWO, the EEOF analysis was applied to the observed 10–20-day filtered OLR anomaly for seven consecutive days. Thus, the EEOF results from day 1 to day 7 represent the half cycle of QBWO events. The region and season for which the EEOF analysis was performed for each QBWO mode were described in Table 1, consistent with those in Kikuchi and Wang (2009). The principal component of the EEOF predicted by the CFSv2 is obtained by projecting the predicted 10–20-day filtered OLR anomalies onto the observed first EEOF of each QBWO mode.

3 Prediction of quasi-biweekly variability

The variance of 10–20-day filtered OLR for NOAA, CFSR, and CFS predictions at lead times of 5, 10, 15, 20, and 25 days in boreal summer and winter are shown in Figs. 1 and 2, respectively. In boreal summer (Fig. 1), large QBW variances appear in the Asian summer monsoon region, the western North Pacific, Central America, and South Pacific. Compared to the results from NOAA OLR data, the CFSR overestimates the QBW variances over the western North Pacific, Central America, and South Pacific, and underestimates the variance in South Asia. The CFS forecast captures the geographical distribution feature of QBW variability, but QBW variances decrease gradually with the increase in lead time.

In boreal winter (Fig. 2), the largest variance of QBW variability can be found in the Australia monsoon–SP convergence zone (SPCZ). Large variance regions also lie in the North Pacific, the South Africa–south Indian Ocean, the North Africa–North Atlantic, and the South America–South Atlantic. Compared to the results based on the NOAA OLR, the CFSR overestimates QBW variability in these regions. In boreal winter, the CFS forecast shows the same problem as in boreal summer, which indicates the weakening of QBW variability with the increase of forecast lead time. In order to assess quantitatively the weakening of the QBW variability with the lead time associated with different QBW modes, we calculated the percent of variance of the 10–20-day filtered OLR forecasted by the CFSv2 with lead times from 1 to 45 days with respect to the initial variance over the eight QBW mode regions defined in Table 1, as shown in Fig. 3. For most modes, the QBW variance decays to near the half of the initial values at the lead times of 11–14 days.

Above analysis indicates the decay of QBWO variance accompanying the increase in forecast lead-time, but cannot reflect the prediction skill at different forecast leads of time. Therefore, temporal correlation between the forecasted and the observed OLR on the time scale of 10–20 days is further calculated at forecast lead times of 6, 9 and 12 days for boreal summer and winter, as shown in Figs. 4 and 5, respectively. In boreal summer (Fig. 4), the prediction skill is lower in the northern hemisphere than in the southern hemisphere. Particularly, the skill decreases to below the 95 % significance level in the AM mode and CA mode regions at the lead time longer than 10 days, while the good skill can be found in the SP mode region even at the lead time beyond 12 days. In boreal winter (Fig. 5), in general, the forecast skill is lower in the southern hemisphere than in the northern hemisphere. At lead time of 9 days, low skills appear in southern Indian Ocean, central western Pacific and South America. At lead time of 12 days, good skills can still be found in the northern hemisphere, but are absent in the southern hemisphere.

Table 1 Eight dominant QBWO modes identified by the EEOF analysis

QBWO mode	Latitudes	Longitudes	Season	Variance explained by EEOF-1 (%)
AM mode	20°S–40°N	30°–180°E	Boreal summer	7.9
CA mode	0°–40°N	20°–160°W	Boreal summer	7.8
SP mode	50°S–5°N	120°–360°E	Boreal summer	6.7
AU–SP mode	50°S–0°	110°E–90°W	Boreal winter	7.5
NP mode	0°–40°N	110°E–80°W	Boreal winter	8.1
NAF mode	0°–50°N	80°W–20°E	Boreal winter	10
SAF mode	40°S–0°	10°–110°E	Boreal winter	8
SAM mode	0°–40°S	0°–80°W	Boreal winter	10.3

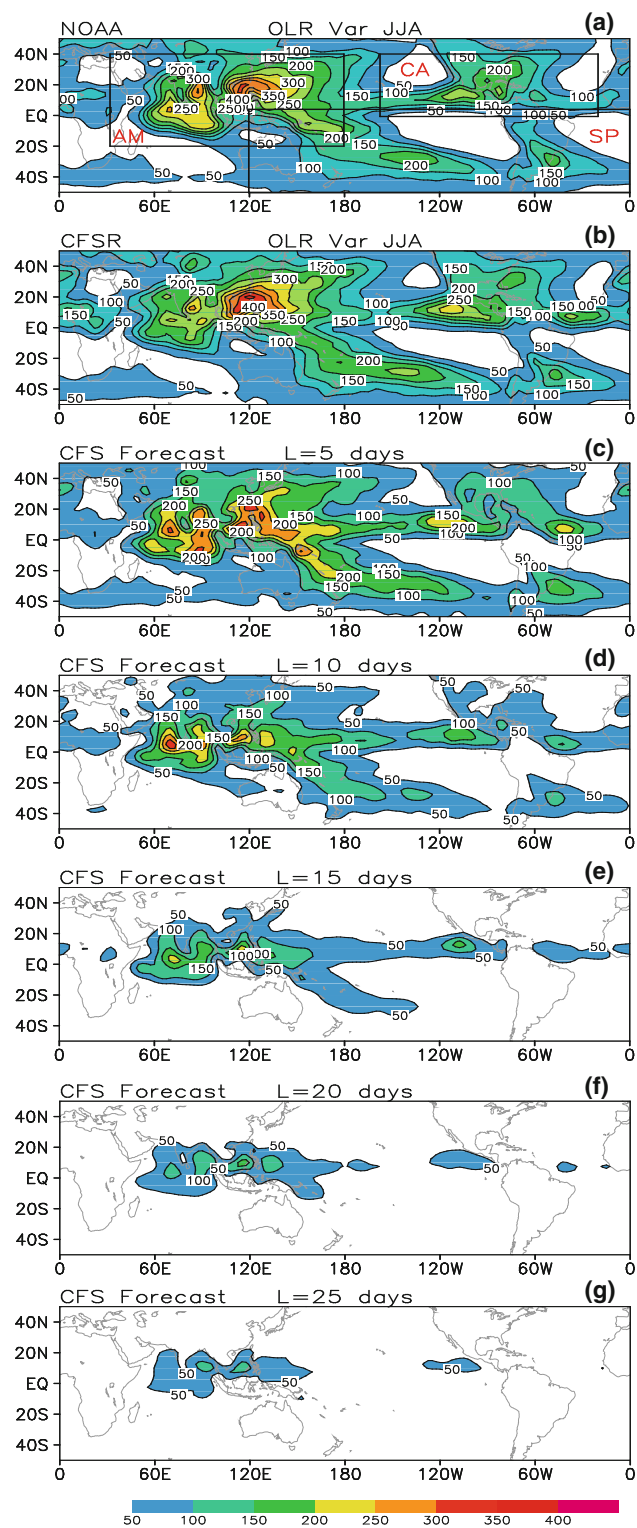


Fig. 1 Variance of 10–20-day filtered OLR (unit: $W^2 m^{-4}$) in boreal summer for NOAA AVHRR (a), CFSR (b), and CFSv2 predictions at lead times of 5, 10, 15, 20, and 25 days (c–g). Solid boxes in a represent regions over which EEOF analyses were performed to identify dominant QBWO modes

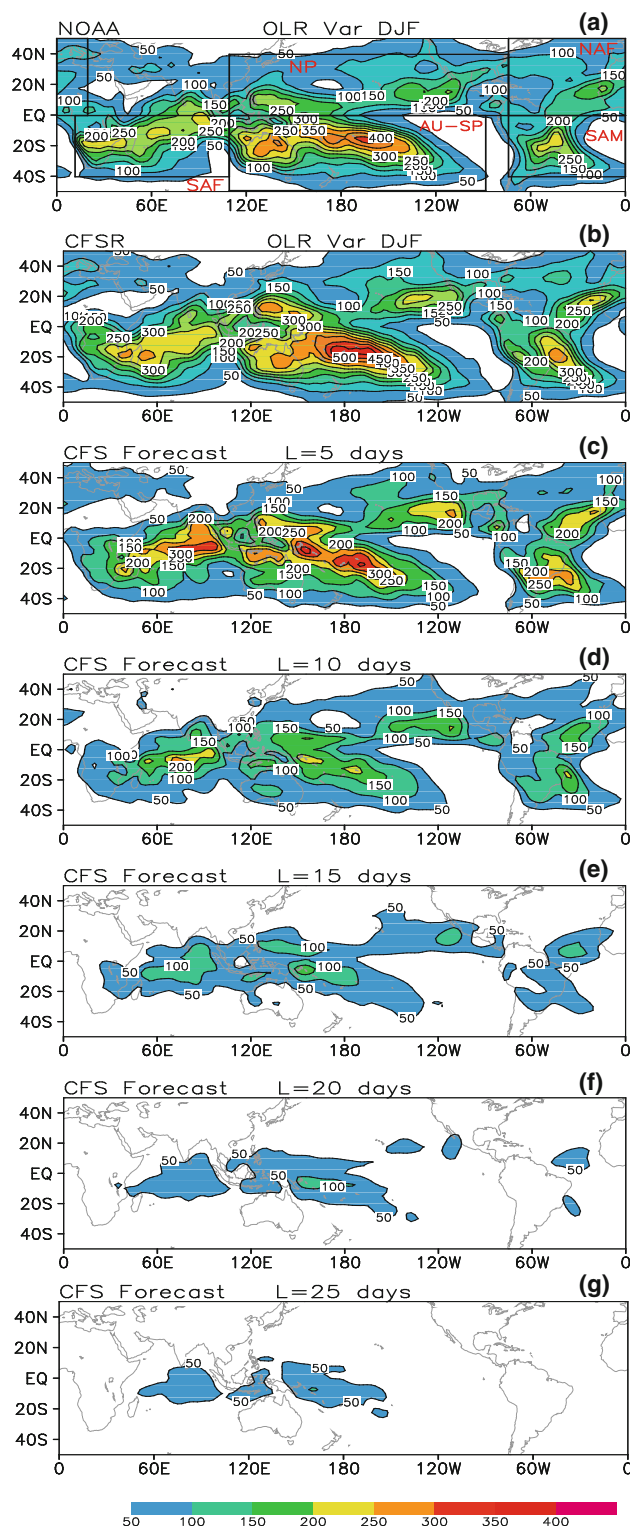


Fig. 2 Same as Fig. 1 but for the OLR in boreal winter

The above results imply that QBW variability has better prediction skills in winter hemisphere than in summer hemisphere in the CFSv2. In particular, the prediction skill

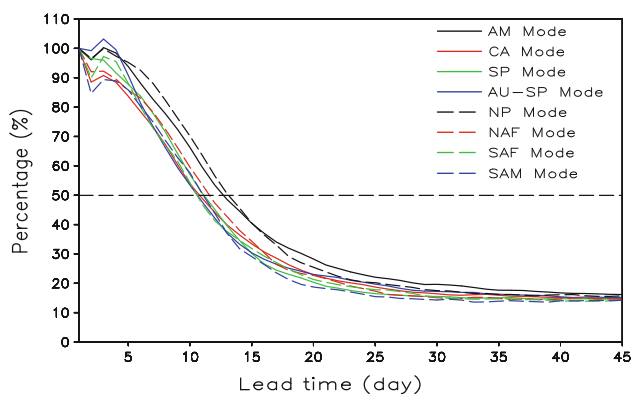


Fig. 3 Percent of variance of the 10–20-day filtered OLR forecasted by the CFSv2 with lead times from 1 to 45 days with respect to the corresponding initial variance for the eight QBWO modes regions (see Table 1)

is lowest in strong monsoon activity regions, such as the Asian monsoon region and North American monsoon region.

4 Prediction skills of the dominant quasi-biweekly oscillation

In Sect. 3, we present a general analysis on the prediction skill of the variability of 10–20-day time scales by the CFSv2 on a global scale. The results indicate that prediction skills show tremendous diversity in different seasons

and over different regions that may be associated with different QBWO modes. Therefore, in this section, we will focus on the prediction skill of the eight dominant QBWO modes defined by the EEOF analysis described in Sect. 2.

Kikuchi and Wang (2009) defined eight QBWO modes in a global perspective using the EEOF-1 mode. Here, we focused on examining the prediction skill of EEOF-1 mode by the CFSv2. Other modes are not considered in the present study. Figure 6 shows the correlation skills for the time series of EEOF-1 of the eight QBWO modes in the CFSv2 with lead times from 1 to 45 days. In general, for most QBWO modes, the skillful forecasts can be obtained with lead times of 10–15 days. Among the eight QBWO modes, the NP mode and SP mode have the highest forecast skills with a useful forecast up to 15 days. The SP mode has a better skill than the NP mode when the lead time is shorter than 13 days. Longer 13 days, the correlation skill is slightly better for the NP mode than for the SP mode. The AM mode and CA mode have the lowest forecast skills with skillful forecasts up to 10 and 11 days, respectively. In addition, among the eight QBWO modes, those modes in winter hemisphere (e.g. SP, NP, and NAF modes) seem to have better forecast skills than those in summer hemisphere (e.g. AM, CA, and SAF modes), which is consistent with the results in Figs. 4 and 5. One may wonder whether the high (low) prediction skill is associated with long (short) auto-correlation for these QBWO modes. We also calculate the lagged auto-correlation for the time series of EEOF-1 of the eight QBWO

Fig. 4 Temporal correlation between the 10–20-day filtered OLR of NOAA AVHRR and those forecasted by the CFSv2at lead times of 6, 9, and 12 days for boreal summer. *Shading areas* are for correlations larger than 0.3 (95 % confidence level)

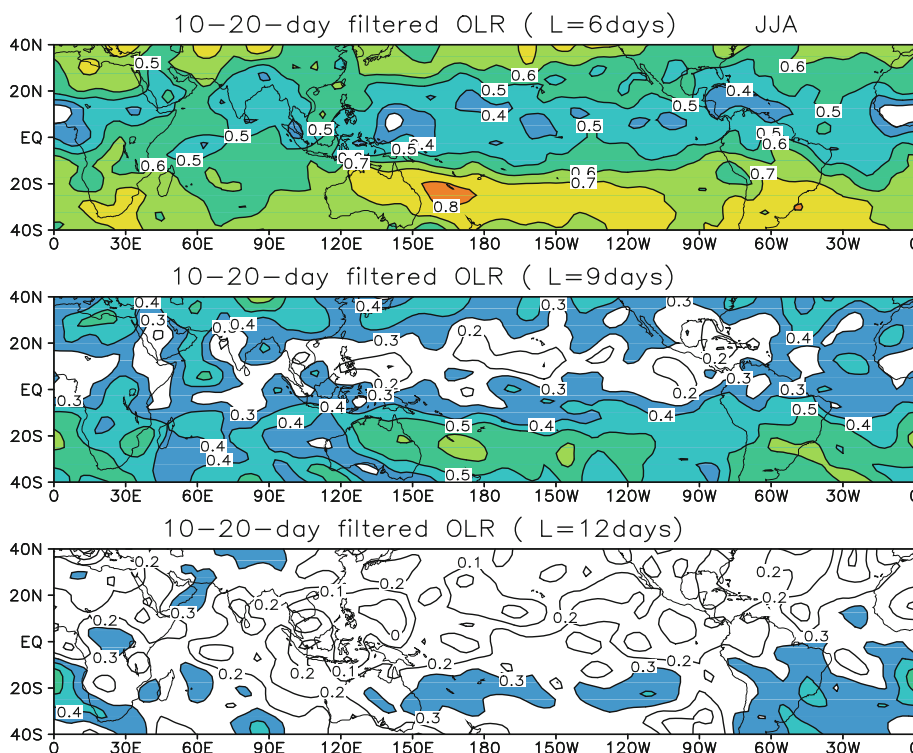
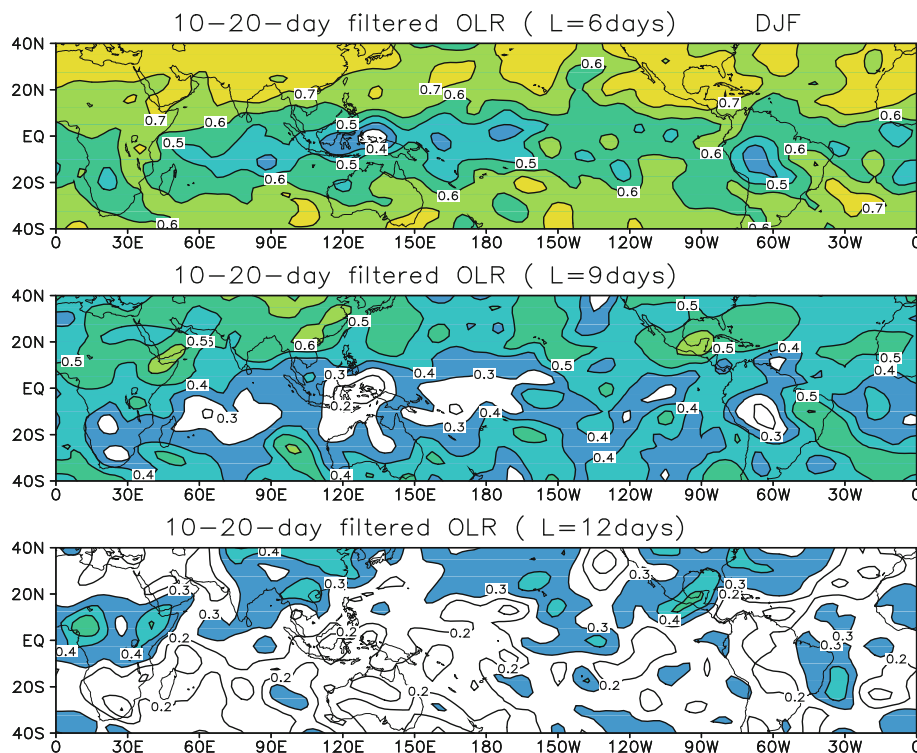


Fig. 5 Same as Fig. 4 but for boreal winter



modes. Result shows that the modes with the highest (lowest) forecast skill may not necessarily have the longest (shortest) auto-correlation, because the differences in lagged auto-correlation of eight modes are very small. Indeed, this result is reasonable because all the modes have the periodicity of quasi-biweekly, and thus at lag time of 4 days (about quarter of one QBWO cycle) the auto-correlation is near zero, and by lagging about 7 days (half cycle) the auto-correlation reaches the minimum.

RMSE and MSSS skills for the time series of EEOF-1 of the eight QBWO modes forecasted by the CFSv2 are presented in Fig. 7. It is evident that the AM mode has the

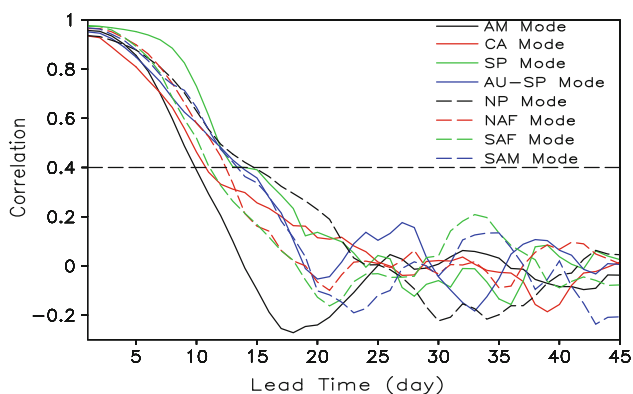


Fig. 6 Correlation skills for the time series of EEOF-1 of the eight QBWO modes predicted by the CFSv2 with lead times from 1 to 45 days. The horizontal dashed line represents correlation skill of 0.4 (95 % confidence level)

largest RMSE during the entire forecast period, while the SP mode has the smallest RMSE at lead times shorter than about 11 days (Fig. 7a). The SP mode has the best MSSS skill and the CA mode has the worst MSSS skill (Fig. 7b).

The above results indicate that the AM and CA modes, which occur in the two most important summer monsoon regions, have the lowest prediction skills among all eight QBWO modes, while the SP mode has the best skill. In the following analysis, we focus on these three modes and further investigate the detailed structure and propagation associated with their lifecycles.

Figure 8 shows the 850-hPa wind and OLR anomalies based on the linear regressions against the time series of EEOF-1 of the AM mode from time lags of 0 to 8 days for observations (CFSR). At day 0, weak enhanced convection emerges in the equatorial central Pacific between 160°E and 180°E and suppressed convection to the west accompanied by an anti-cyclonic circulation, resembling a Rossby wave response. In the meantime, a weak enhanced convection band appears over southern Japan, northern SCS, and central Indian Ocean. From day 2 to day 8, enhanced convection over equatorial central Pacific strengthens and propagates northwestward into the SCS accompanied by strengthened cyclonic circulation response. Meanwhile, the suppressed convection to its west also propagates northwestward, reaches its mature phase over the SCS during day 2 and day 4, then weakens and shifts into the Indian Ocean. At day 6, a new center of suppressed convection appears in the equatorial central

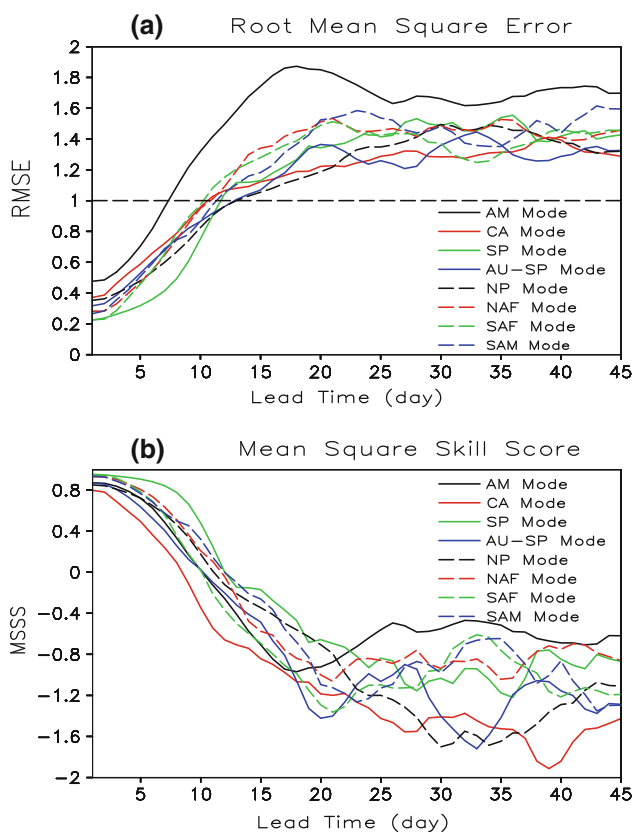


Fig. 7 RMSE (a) and MSSS (b) skills for the time series of EEOF-1 of eight the QBWO modes from the CFSv2 with lead times from 1 to 45 days. In a, the horizontal line represents the RMSE skill of 1. a Root mean square error, b mean square skill score

Pacific displacing the enhanced convection at day 0. Also, noteworthy is that the enhanced convection band appears over the Southern China at days 2 and 4 indicating a strong Mei-yu and Baiu fronts.

Figure 9 displays the lifecycle of the CA mode. At day 0, an enhanced convection anomaly emerges in the eastern tropical Atlantic. To its west are suppressed convection, enhanced convection, and suppressed convection, alternatively, accompanied by anti-cyclonic, cyclonic and anti-cyclonic circulation to the northwest of the convection anomalies. From day 2 to day 8, these convection centers and corresponding cyclonic and anticyclonic circulations move northwestward. The westernmost convection and circulation cell finally disappears in the eastern Pacific. These results are consistent with the study by Kikuchi and Wang (2009).

To compare the structure and propagation of QBWO predicted by the CFSv2 with the observations, Fig. 10 displays the linear regressions of forecasted 850-hPa wind and OLR anomalies by the CFSv2 at lead times of 2, 4, 6, 8, and 10 days against the time series of EEOF-1 of the observed AM mode. Actually, Fig. 10 reflects the structure of the AM mode at day 0 (Fig. 8a) predicted by the CFSv2

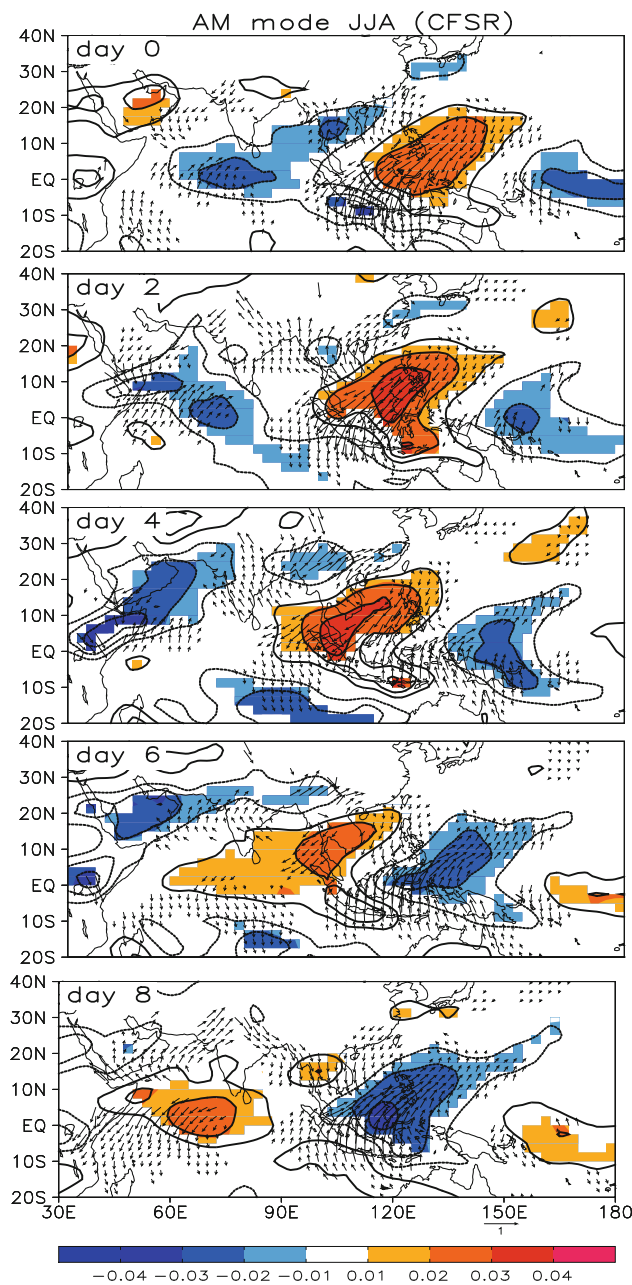


Fig. 8 Linear regressions of boreal summer 850-hPa wind anomalies ($m s^{-1}$; vectors) and OLR anomalies ($W m^{-2}$; shadings and contours) against the time series of EEOF-1 of the AM mode from time lag 0 to 8 days for observations (CFRR). Only the wind vectors that significantly exceed the 95 % confidence level are shown. Contour interval for OLR is $0.01 W m^{-2}$ and values that significantly exceed the 95 % confidence level are shaded

at different lead times. Compared to the observations, at lead time of 2 days, the CFSv2 well captures the structure of convection and circulation associated with QBWO, including the enhanced convection band extending from southern Japan to northern SCS and central Indian Ocean, the suppressed convection to the east of Philippines with slightly larger amplitude, and the weak enhanced

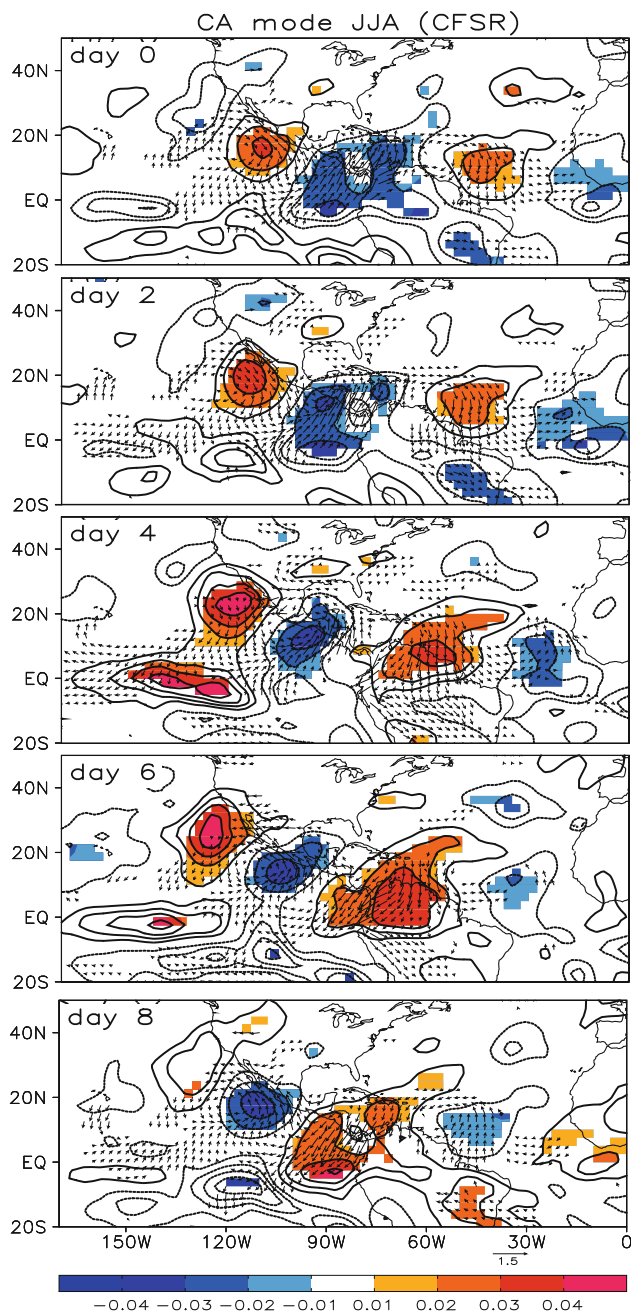


Fig. 9 Linear regressions of boreal winter 850-hPa wind anomalies (m s^{-1} ; vectors) and OLR anomalies (W m^{-2} ; shadings and contours) against the time series of EEOF-1 of the CA mode from time lag 0 to 8 days for observations (CFSR). Only the wind vectors that significantly exceed the 95 % confidence level are shown. Contour interval for OLR is 0.01 W m^{-2} and values that significantly exceed the 95 % confidence level are shaded

convection near the central Pacific which is the origin region of QBWO of the AM mode. These characteristics are also predicted by the CFSv2 at lead times up to 10 days. However, two deficiencies are also obvious. One is that the amplitudes of QBWO decrease with the increase in the forecast lead time, which is consistent with the

results in Fig. 3. The other is that, compared to the observations, the forecasted convection and circulation shift eastward with the increase in lead time, which indicates a slower propagating speed. Similar problems can also be found in the forecast of the CA mode as shown in Fig. 11. In particular, both the enhanced convection over the Caribbean Sea and the suppressed convection over the central Atlantic present a northeastward shift with the increase in lead time, while the convection cells over the southwestern America have no obvious shift. Thus, the forecasted structure of the CA mode seems to be more in disorder than that of the AM mode. For the AM and CA modes, the eastward shift in structure forecasted by the CFSv2 is displayed more clearly in Fig. 12. For the AM mode, the eastward shift of QBWO convection occurs over the whole AM region. A rough estimate of the speed is about 2.5 longitudes/day. Beyond 10 days, the CFSv2 fails to predict the observed QBWO phase. For the CA mode, the eastward shift is weaker than that of the AM mode.

As mentioned above, among the eight QBWO modes, the SP mode has the best prediction skill. Figure 13 shows the linear regressions of 850-hPa wind anomalies and OLR anomalies in the observations from time lag 0 to 8 days against the time series of EEOF-1 of the SP mode. Unlike the AM and CA modes, the SP mode occurs in winter hemisphere and is characterized by an eastward propagating Rossby wave train extending from New Guinea to southern Brazil (Fig. 13). Shown in Fig. 14 are the forecasts by the CFSv2 at lead times of 2, 4, 6, 8, 10 days. The CFSv2 well captures the structure of the SP mode. Moreover, compared to the AM and CA modes, no obvious phase shift can be found with the increase in the lead time, which is more clearly seen in a longitude-lead time diagram shown in Fig. 15. The CFSv2 can obtain skillful predictions beyond 10 days, and there is no obvious phase bias when the lead time is shorter than 15 days. The results indicate that the propagating speed of the SP mode in the CFSv2 is more realistic than that of the AM mode, which contributes to the better prediction skill for the SP mode.

5 Discussions

The dominant QBWO modes tend to occur over different regions and be associated with the global monsoons (Kikuchi and Wang 2009). In a monsoon region, there also exists strong air–sea interaction on subseasonal time scales, particularly in the tropical Indo-western Pacific (Hendon and Glick 1997; Waliser et al. 1999; Woolnough et al. 2000; Kembell-Cook and Wang 2001; Fu et al. 2003; Wu et al. 2008). However, most of these studies focused on the 20–60-day time scales, except for Wu et al. (2008). A discussion of the local air–sea interaction on the 10–20-day

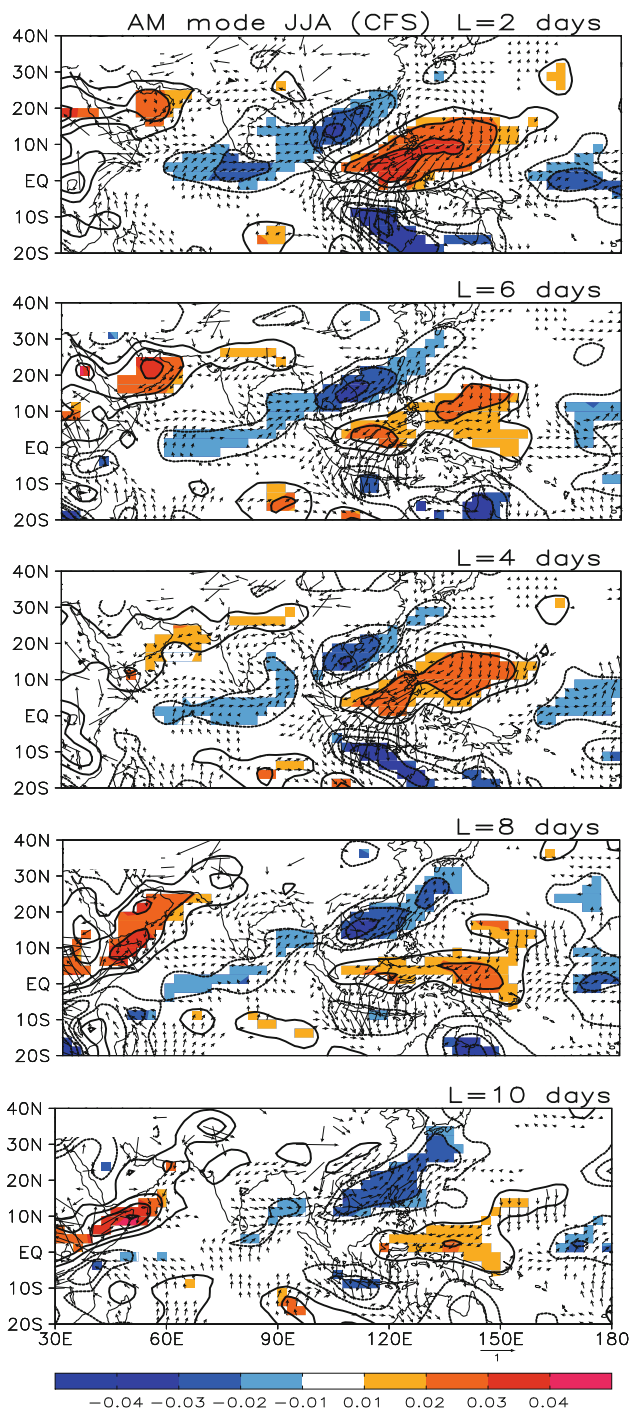


Fig. 10 Linear regressions of forecasted 850-hPa wind anomalies (m s^{-1} ; *vectors*) and OLR anomalies (W m^{-2} ; *shadings* and *contours*) by the CFSv2 at lead times of 2, 4, 6, 8, and 10 days against the time series of EEOF-1 of the observed AM mode in boreal summer. Only the wind vectors that significantly exceed the 95 % confidence level are shown. *Contour* interval for OLR is 0.01 W m^{-2} and values that significantly exceed the 95 % confidence level are *shaded*

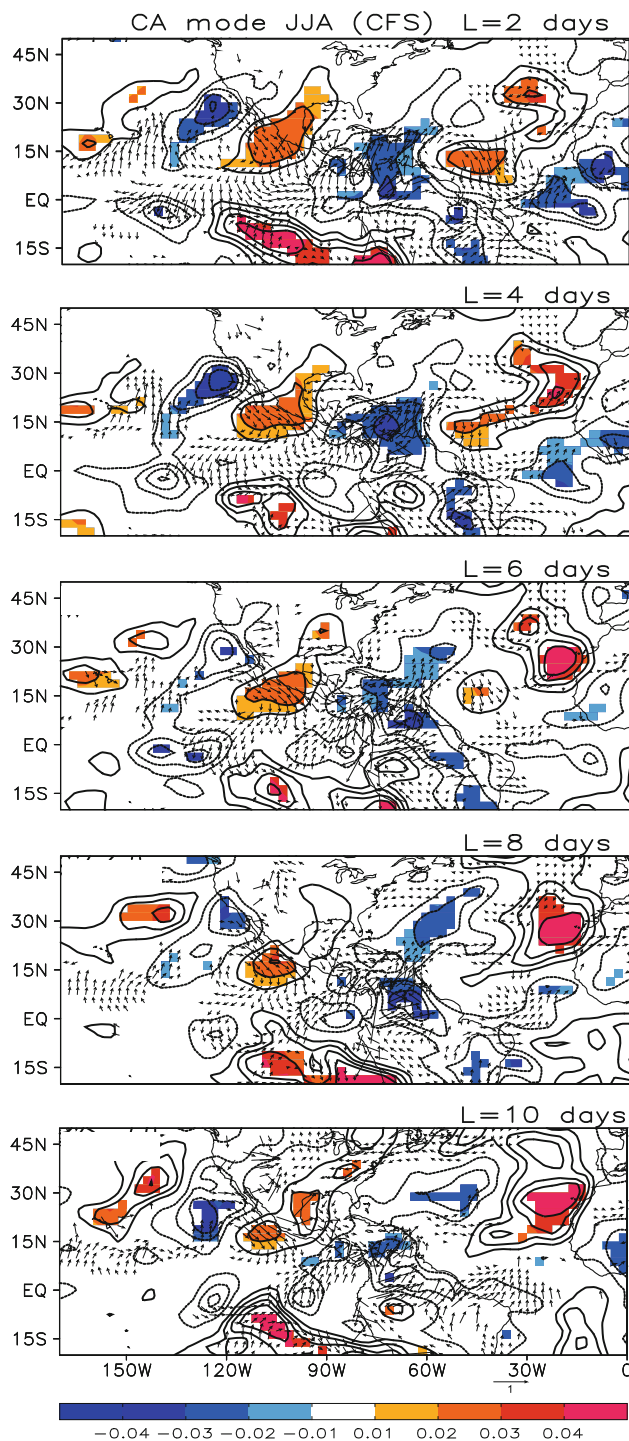


Fig. 11 Linear regressions of forecasted 850-hPa wind anomalies (m s^{-1} ; *vectors*) and OLR anomalies (W m^{-2} ; *shadings* and *contours*) by the CFSv2 at lead times of 2, 4, 6, 8, and 10 days against the time series of EEOF-1 of the observed CA mode in boreal summer. Only the wind vectors that significantly exceed the 95 % confidence level are shown. *Contour* interval for OLR is 0.01 W m^{-2} and values that significantly exceed the 95 % confidence level are *shaded*

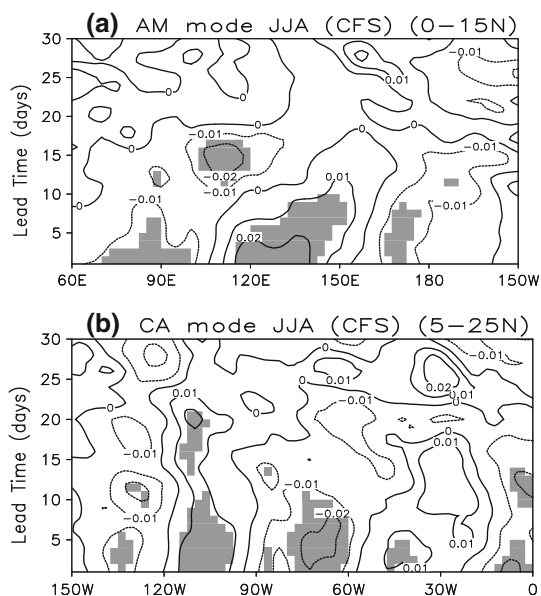


Fig. 12 Longitude–lead time diagrams of the regressions of OLR anomalies (W m^{-2}) forecasted by the CFSv2 with lead times from 1 to 30 days onto the time series of EEOF-1 of the observed AM mode (**a** along 0° – 15°N) and CA mode (**b** along 5° – 25°N). Values significantly exceeding the 95 % confidence level are shaded. **a** AM mode JJA (CFS) (0° – 15°N). **b** CA mode JJA (CFS) (5° – 25°N)

time scales may be helpful for understanding the difference in prediction skill of different QBWO modes.

Figure 16 shows the lead-lag correlations between 10- and 20-day filtered precipitation and SST for observations, which reflects the air–sea interaction on the 10–20-day time scales. Daily SST data are the surface temperature data from the NCEP CFSR and the same period as the CFSv2 forecast from 1999 to 2010 is used. It can be found that the intensity of air–sea coupling strongly depends on the season with the most prominent interaction in the summer hemisphere. In summer, as shown in Fig. 16a, the strong air–sea interaction occurs in the Asian monsoon region, African monsoon region and North American monsoon region in the Northern Hemisphere. The strongest interaction occurs in the tropical Indo-western Pacific. In the Asian monsoon region, positive correlation appears when SST anomalies lead precipitation anomalies with the maximum exceeding 0.4. Significant negative correlation appears when SST anomalies lag anomalous precipitation with the maximum exceeding 0.5. The time lag also shows notable spatial variations. The lead time for SST significantly correlating with precipitation is slightly shorter in the Arabian Sea and the western Pacific than in the Bay of Bengal and SCS, and the corresponding lag time is longer in the western Pacific than in the Bay of Bengal and SCS. These results are very similar to the study by Wu et al. (2008), though broader time scales are included in the data they used. Additionally, the characteristics of the lead and

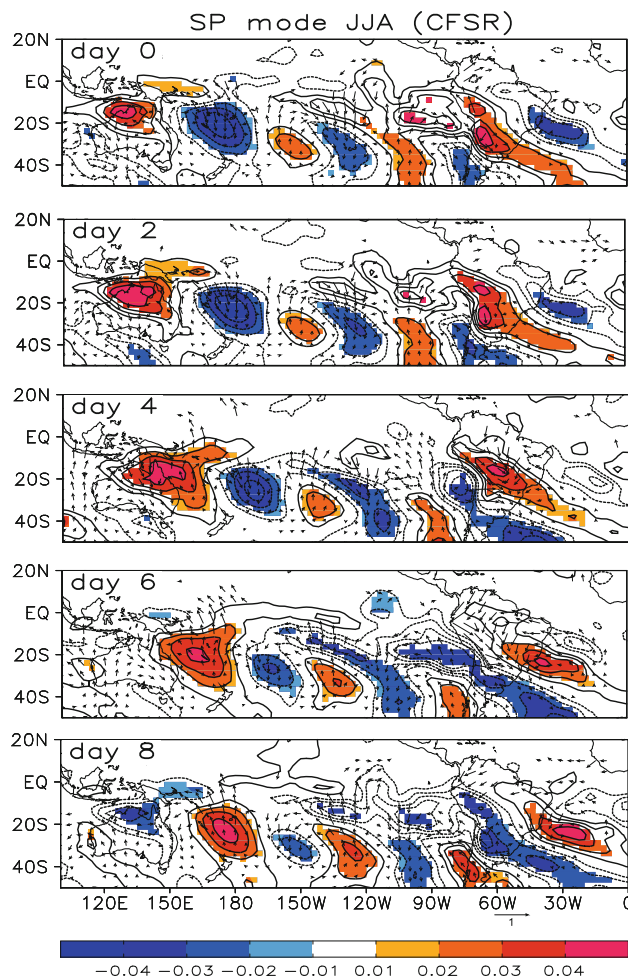


Fig. 13 Linear regressions of boreal summer 850-hPa wind anomalies (m s^{-1} ; vectors) and OLR anomalies (W m^{-2} ; shadings and contours) for observations (CFSR) from time lag 0 to 8 days against the time series of EEOF-1 of the SP mode. Only the wind vectors that significantly exceed the 95 % confidence level are shown. Contour interval for OLR is 0.01 W m^{-2} and values that significantly exceed the 95 % confidence level are shaded

lag times are also consistent with Wu et al. (2008), which is shorter than those obtained from the 20–60-day band-pass filtered data (Hendon and Glick 1997; Waliser et al. 1999; Woolnough et al. 2000; Kemball-Cook and Wang 2001; Fu et al. 2003). Compared to the Northern Hemisphere, the lead and lag correlations are much weaker in the Southern Hemisphere (Fig. 16b). Similarly, in winter, they are also much weaker in the Northern Hemisphere than those in the Southern Hemisphere (Figs. 16c, d). The results indicate that, for those QBWO modes in summer hemisphere, particularly in the monsoon regions, the air–sea interaction on the 10–20-day time scales perhaps plays a more important role in maintaining QBWO.

Examining the air–sea interaction on the 10–20 day time scales in the CFSv2 is helpful for understanding the forecasted QBWO by the CFSv2. Here, we calculate the lead-

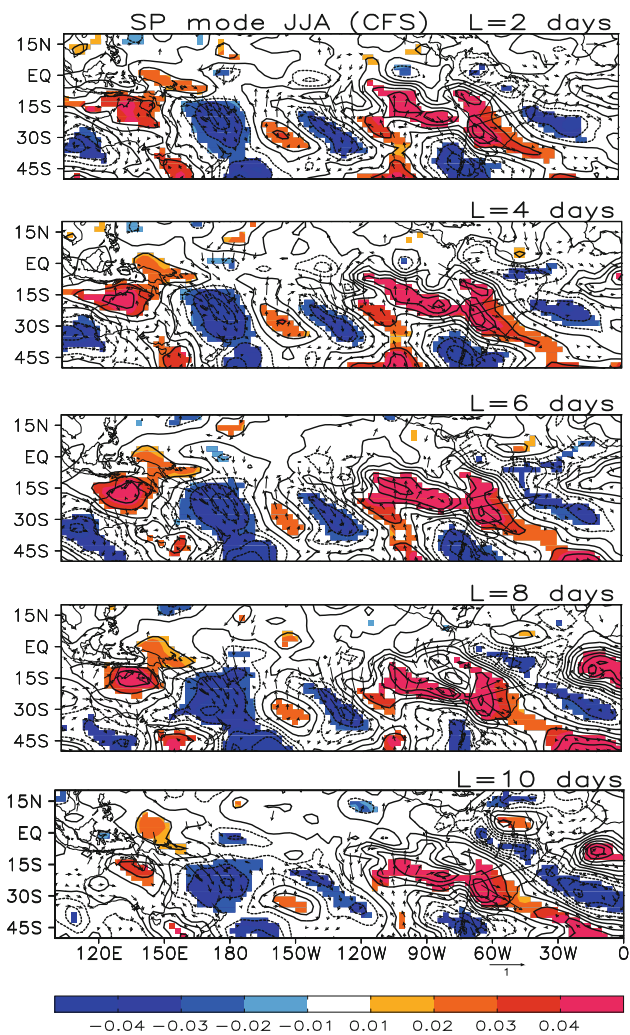


Fig. 14 Linear regressions of the forecasted boreal summer 850-hPa wind anomalies (m s^{-1} ; vectors) and OLR anomalies (W m^{-2} ; shadings and contours) by the CFSv2 at lead times of 2, 4, 6, 8, and 10 days against the time series of EEOF-1 of the observed SP mode. Only the wind vectors that significantly exceed the 95 % confidence level are shown. Contour interval for OLR is 0.01 W m^{-2} and values that significantly exceed the 95 % confidence level are shaded

lag correlations between 10- and 20-day band-pass filtered precipitation and surface temperature averaged over the regions associated with the eight QBWO modes forecasted by the CFSv2 with lead times from 1 to 45 days, as shown in Fig. 17. For the five summer hemisphere modes (AM, CA, Au-SP, SAF, and SAM modes), there exists obvious air-sea interaction on the 10–20-day time scales. However, it weakens rapidly with the increase of lead time except for the SAM mode. For the SAM mode, the strong air-sea interaction can maintain much longer, which may contribute to the relatively higher forecast skill than the other four modes. For the winter hemisphere modes (SP, NAF, and NP modes), which can be better forecasted than those summer modes, however, air-sea interaction seems much weaker, consistent with the observation shown in Fig. 16.

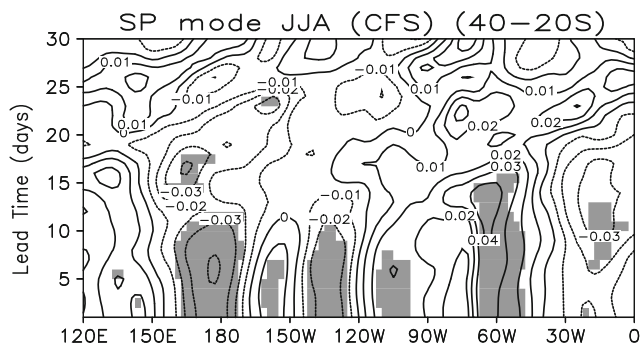


Fig. 15 Longitude-lead time diagram of the regressions of boreal summer OLR anomalies (W m^{-2}) forecasted by the CFSv2 with lead times from 1 to 30 days onto the time series of EEOF-1 of the observed SP mode along 40° – 20° S. Values significantly exceeding the 95 % confidence level are shaded

This feature indicates that air-sea interaction is perhaps less crucial for prediction of winter hemisphere modes.

ENSO is the most important climate phenomenon as a result of air-sea interaction on the inter-annual time scales. Different ENSO phases provide different air-sea backgrounds. Thus, the predictability of QBWO may be different in different ENSO phases. From 1999 to 2010, there were three El Niño summers (2002, 2004, and 2009), four El Niño winters (2002/2003, 2004/2005, 2006/2007, and 2009/2010), three La Niña summers (1999, 2000, and 2010), and four La Niña winters (1999/2000, 2000/2001, 2005/2006, and 2007/2008) based on the SST anomalies in the Niño 3.4 region. Shown in Fig. 18 are the prediction skills of the eight QBWO modes in El Niño and La Niña years, respectively. Although only limited samples can be used for composite due to the short forecast data, it is very interesting that most modes, except for the NP and NAF modes, have better forecast skills in the El Niño years than in the La Niña years in the CFSv2. We speculate that the modulation of the global monsoons by ENSO might alter the predictability of QBWO. Further analysis of observations and modeling studies are required to understand the impact of ENSO on the predictability of QBWO.

On the other hand, different QBWO modes involve different dynamic mechanisms, which may influence the prediction by numerical models. The phenomena of QBWO mainly occur in the tropical monsoon region and the mid-latitude westerly zone (Wu and Li 1990). Surface hydrological effects, condensation heating, and wave-flow interaction (Webster 1983; Wu and Luo 1987; Wu and Li 1990) are considered important to the QBWO dynamics. For tropical monsoon low-frequency variability, the surface hydrological effects and the forcing from the mid-high latitude disturbances are both important (Webster 1983; Wu and Luo 1987; Wu and Li 1990). For the mid-latitude low-frequency variability, the wave-flow interaction may be important (Wu and Li 1990). According to Kikuchi and

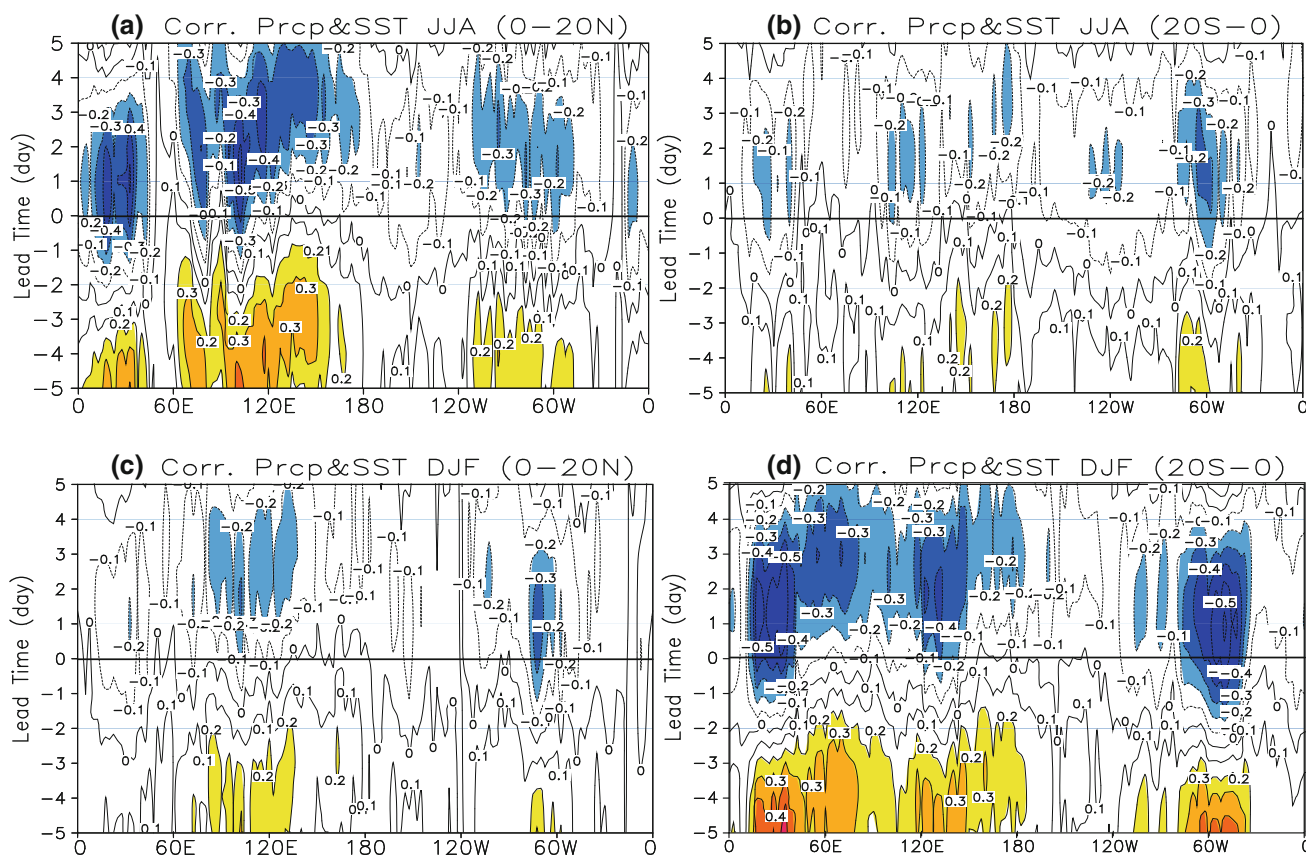


Fig. 16 Lead-lag correlations between 10- and 20-day band-pass filtered precipitation and SST from the CFSR for summer along 0°–20°N (a) and 20°S–0 (b), and for winter along 0°–20°N (c) and 20°S–0 (d). Correlations are contoured every 0.1 and values larger than 0.2

are shaded. Negative (positive) lead days represent that SST leads (lags) precipitation. **a** Corr. Prcp and SST JJA (0°–20°N). **b** Corr. Prcp and SST JJA (20°S–0). **c** Corr. Prcp and SST DJF (0°–20°N). **d** Corr. Prcp and SST DJF (20°S–0)

Wang (2009), the eight QBWO modes examined in this paper include westward-propagating modes (e.g. AM and CA modes) and eastward-propagating modes (e.g. SP, AU–SP, and SAM modes). The westward-propagating modes can be understood in terms of equatorial Rossby waves in the presence of monsoon mean flow and convective coupling, while the eastward-propagating modes are connected with upstream extratropical Rossby wave trains (Kikuchi and Wang 2009). Therefore, the extratropical wave-flow interaction is perhaps important for those eastward-propagating modes. The eastward-propagating modes (e.g. SP, AU–SP, and SAM modes) also seem to be better predicted than the westward-propagating modes (e.g. AM and CA modes) in the CFSV2, which is perhaps partially due to the fact that the tropical QBWO modes involve complicated interaction of tropical and extra-tropical dynamics. Meanwhile, as indicated in Sect. 4, winter modes seem to have better forecast skill than summer modes, which may also be due to the stronger wave-flow interaction in mid-latitude in winter than in summer. Further studies are needed to understand the dynamical mechanism of different QBWO modes.

Finally, it should be pointed out that, in the present paper, we focused on the prediction skills of eight quasi-biweekly modes identified by the first EEOF modes. Most EEOF1 modes can explain variances no more than 10 % as shown in Table 1. However, the EEOF modes are paired, and the first two EEOF modes have similar structure but with a difference in phase because QBW oscillations are propagating modes. Consequently, for most QBW modes, the total variances explained by the first two EEOF modes exceed 10 % even approaching 20 % for paired modes. Nevertheless, the QBW variations can only explain part of the total variability of the atmosphere, and so increasing the prediction skill of the QBWO does not necessary improve the whole forecast. However, as one of important intra-seasonal components, it is important for operational models to forecast QBWO skillfully.

6 Summary

In this study, we have examined the prediction skill of the atmospheric variability on quasi-biweekly time scales

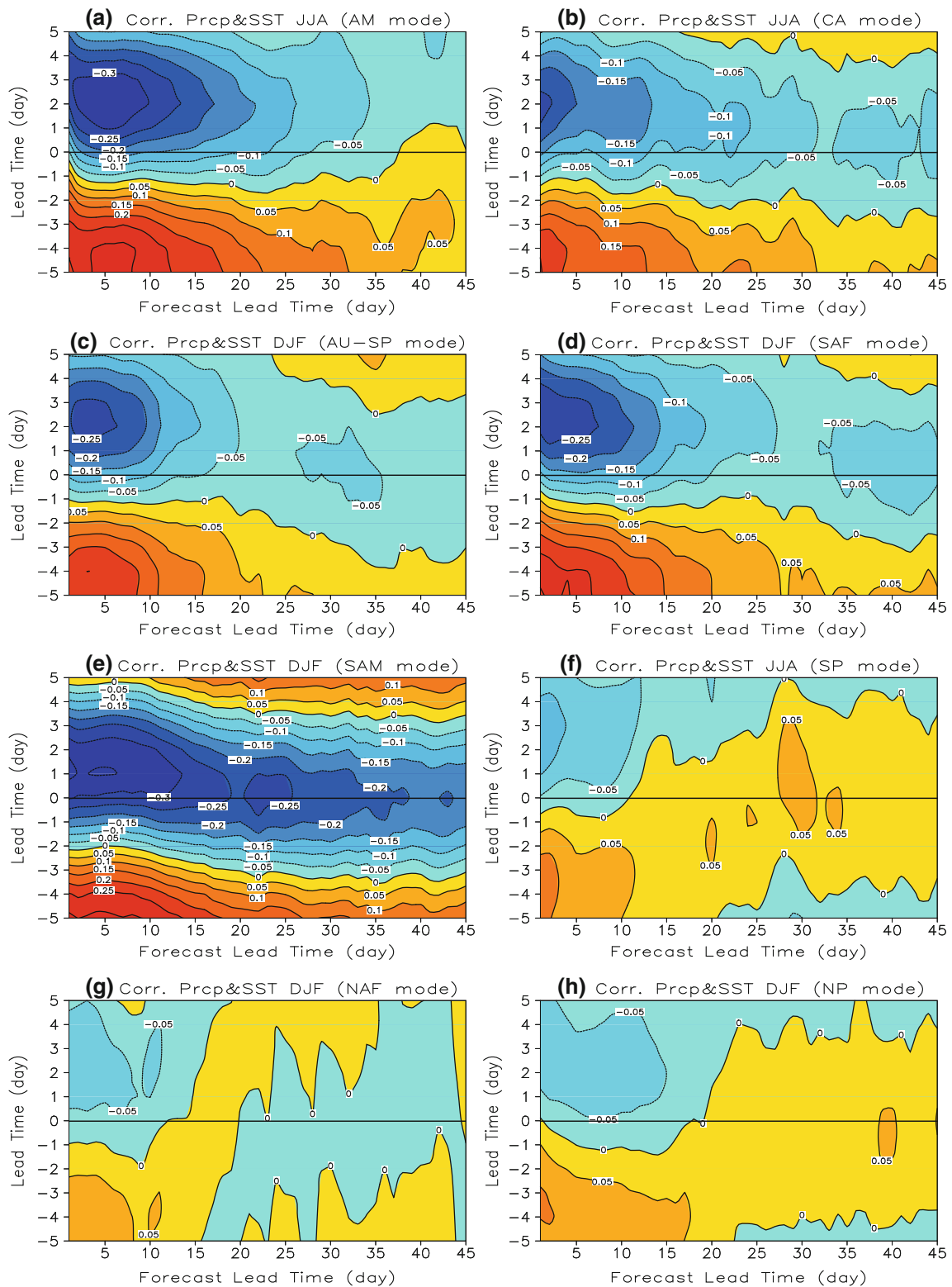


Fig. 17 Lead-lag correlations between 10- and 20-day band-pass filtered precipitation and SST averaged over the regions associated with the eight QBWO modes (see Table 1) forecasted by the CFSv2 with lead times from 1 to 45 days. *Negative (positive)* lead days represent that SST leads (lags) precipitation. **a** Corr. Prcp and SST

JJA (AM mode), **b** corr. Prcp and SST JJA (CA mode), **c** corr. Prcp and SST DJF (AU-SP mode), **d** corr. Prcp and SST DJF (SAF mode), **e** corr. Prcp and SST DJF (SAM mode), **f** corr. Prcp and SST JJA (SP mode), **g** corr. Prcp and SST DJF (NAF mode), **h** corr. Prcp and SST DJF (NP mode)

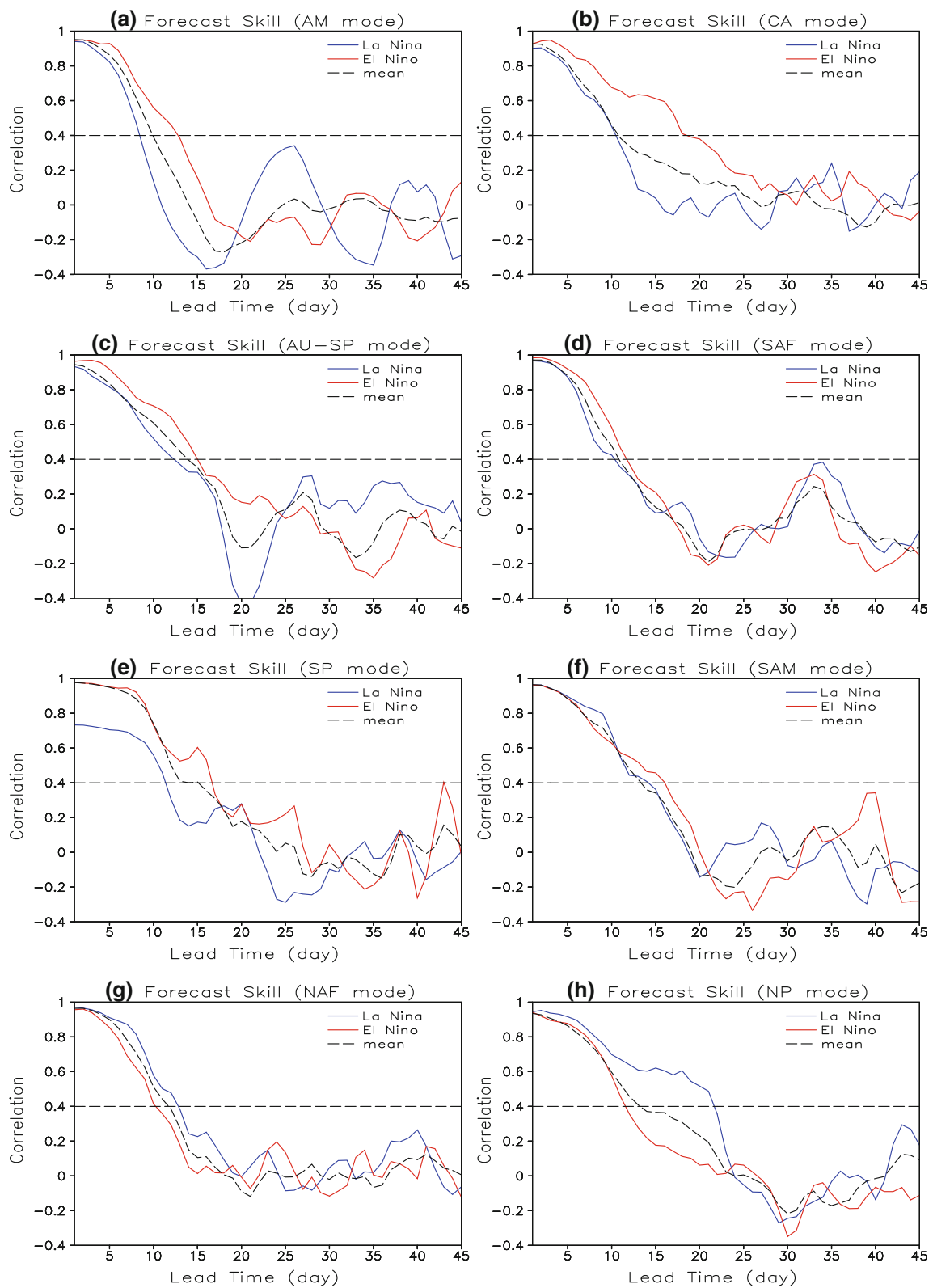


Fig. 18 Correlation skills for the time series of EEOF-1 of the eight QBWO modes predicted by the CFSv2 with lead times from 1 to 45 days for El Nino years (red line), La Nina years (blue line) and 12-years mean (dashed line). The horizontal lines represent correlation

skill of 0.4 (95 % confidence level). **a** Forecast skill (AM mode), **b** forecast skill (CA mode), **c** forecast skill (AU-SP mode), **d** forecast skill (SAF mode), **e** forecast skill (SP mode), **f** forecast skill (SAM mode), **g** forecast skill (NAF mode), **h** forecast skill (NP mode)

using the retrospective forecasts by the NCEP CFSv2. Particularly we focused on the eight dominant QBWO modes identified by the EEOF analysis. Among them, there are three boreal summer modes (AM, CA, and SP modes) and five austral summer modes (AU–SP, SAF, SAM, NP, and NAF modes). In all QBWO regions, 10–20-day's variances decrease with the increase of the forecast lead time, and in general, reduce to only the half of their initial values at the lead times of 11–14 days. The CFSv2 has better prediction skills for the QBW variability in winter hemisphere than in summer hemisphere. The prediction skill is lowest in strong active monsoon regions (e.g. Asian monsoon and North American monsoon).

Following Kikuchi and Wang (2009), eight dominant QBWO modes are extracted by the EEOF analysis. The first principal component of the EEOF analysis for the eight QBWO modes is taken as the QBWO index and its prediction by the CFSv2 is further quantitatively assessed. In general, skillful forecasts can be obtained at the lead times of 10–15 days for most QBWO modes. Those modes in winter hemisphere (e.g. SP, NP, and NAF modes) seem to have the better forecast skills than those in summer hemisphere (e.g. AM, CA, and SAF modes) associated with stronger monsoon activity. Among the eight QBWO modes, the NP and SP modes have the best forecast skills with a useful forecast up to 15 days and the AM and CA modes, occurring in the two most important summer monsoon region, have the lowest forecast skills with skillful forecasts only up to 10 and 11 days, respectively. The AM mode has the largest RMSE during the whole forecast period among the eight QBWO modes while the SP mode has the smallest RMSE. The structures and propagation of the AM, CA and SP mode predicted by the CFSv2 are further analyzed and compared with the observations to explain the significant difference in prediction skill. For the AM and CA modes, as compared to the observations, the forecasted QBWO phase shows an obvious eastward bias with the increase of the lead time, particularly for the AM mode with a speed of 2.5 longitudes/day, which indicates a slower propagating speed than the observations because both the AM and CA mode are westward propagating modes. There is no obvious phase bias for the SP mode when the lead time is shorter than 15 days, which indicates that the propagating speed of the SP mode in the CFSv2 is more realistic than that of the AM mode, which contributes to the better prediction skill for the SP mode.

For better understanding the difference in prediction skill among different QBWO modes, we discussed the possible influences of air–sea interaction on 10–20-day and interannual time scales on the prediction. The observational analysis shows that the local air–sea interaction on the 10–20-day time scales is stronger in the summer hemisphere, which indicates that for those QBWO modes

in summer hemisphere, particularly in monsoon regions, the air–sea interaction on the 10–20-day time scales perhaps plays a more important role. In the CFSv2 prediction, there also exists strong air–sea interaction on the 10–20-day time scales in the five summer hemisphere modes (AM, CA, Au–SP, SAF, and SAM modes), while absent in the winter hemisphere modes. However, the local air–sea coupling weakens rapidly with the increase of forecast lead time in the CFSv2 associated with the SAM mode. For the QBWO modes in the winter hemisphere (SP, NAF, and NP modes), the air–sea interaction may not be crucial. Consequently, these QBWO modes can possibly be better forecasted by the model than those summer modes. The prediction skills of the eight QBWO modes are also compared between El Niño years and La Niña years. It is interesting to note that most QBWO modes, except for the NP and NAF modes, have better forecast skills in El Niño years than in La Niña years in CFSv2. Further studies are needed to understand the impact of ENSO on the predictability of QBWO. Different dynamical mechanisms for the QBWO modes may be partially responsible for the differences in prediction skill among different QBWO modes.

Acknowledgments This research was supported by grants from the National Basic Research Program of China (973 Program, 2012CB955902), the National Natural Science Foundation of China (40905035), Zhongshan University “985 Project” Phase 3 and the Key Technologies R&D Program of China (2009BAC51B05).

References

- Agudelo PA, Hoyos CD, Webster PJ, Curry JA (2009) Application of a serial extended forecast experiment using the ECMWF model to interpret the predictive skill of tropical intraseasonal variability. *Clim Dyn* 32:855–872
- Chen TC, Chen JM (1993) The 10–20-day mode of the 1979 Indian monsoon: its relation with the time variation of monsoon rainfall. *Mon Weather Rev* 121:2465–2482
- Chen TC, Chen JM (1995) An observational study of the South China Sea monsoon during the 1979 summer: onset and life cycle. *Mon Weather Rev* 123:2295–2318
- Chen TC, Yen MC, Weng SP (2000) Interaction between the summer monsoons in East Asia and the South China Sea: intraseasonal monsoon modes. *J Atmos Sci* 57:1373–1392
- Duchon CE (1979) Lanczos filtering in one and two dimensions. *J Appl Meteorol* 18:1016–1022
- Fu X, Wang B, Li T, McCreary JP (2003) Coupling between northward-propagating intraseasonal oscillations and sea surface temperature in the Indian Ocean. *J Atmos Sci* 60:1733–1753
- Fukutomi Y, Yasunari T (1999) 10–25 day intraseasonal variations of convection and circulation over East Asia and western North Pacific during early summer. *J Meteorol Soc Jpn* 77:753–769
- Fukutomi Y, Yasunari T (2002) Tropical–extratropical interaction associated with the 10–25 day oscillation over the western Pacific during the northern summer. *J Meteorol Soc Jpn* 80:311–331
- Goswami BN, Ajayamohan RS, Xavier PK, Sengupta D (2003) Clustering of synoptic activity by Indian summer monsoon intraseasonal oscillations. *Geophys Res Lett* 30:1431. doi:10.1029/2002GL016734

- Gottschalck J, Wheeler M, Weickmann K, Vitart F, Savage N, Lin H, Hendon H, Waliser D, Sperber K, Prestrelo C, Nakagawa M, Flatau M, Higgins W (2010) A framework for assessing operational model MJO forecasts: a project of the CLIVAR Madden-Julian oscillation working group. *Bull Am Meteorol Soc* 91(8):1247–1258
- Hendon HH, Glick J (1997) Intraseasonal air–sea interaction in the tropical Indian and Pacific oceans. *J Clim* 10:647–661
- Jia X, Yang S (2013) Impacts of the quasi-biweekly oscillation over the western North Pacific on East Asian subtropical monsoon during early summer. *J Geophys Res* 118. doi:10.1002/jgrd.50422
- Jiang X, Lau NC (2008) Intraseasonal teleconnection between North American and western North Pacific monsoons with 20-day time scale. *J Clim* 21:2664–2678
- Jiang X, Waliser DE (2009) Two dominant subseasonal variability modes of the eastern Pacific ITCZ. *Geophys Res Lett* 36:L04704. doi:10.1029/2008GL036820
- Kemball-Cook S, Wang B (2001) Equatorial waves and air–sea interaction in the boreal summer intraseasonal oscillation. *J Clim* 14:2923–2942
- Kikuchi K, Wang B (2009) Global perspective of the quasi-biweekly oscillation. *J Clim* 22:1340–1359
- Kiladis GN, Hall-McKim EA (2004) Intraseasonal modulation of precipitation over the North American monsoon region. In: *Proceedings of the 15th symposium on global change and climate variations*, Seattle, WA. Available online at <http://ams.confex.com/ams/pdfpapers/72428.pdf>
- Krishnamurti TN, Ardanuy P (1980) 10 to 20-day westward propagating mode and “breaks in the monsoons”. *Tellus* 32:15–26
- Li CY, Zhou W, Chan JCL, Huang P (2012) Asymmetric modulation of the Western North Pacific cyclogenesis by the Madden-Julian Oscillation under ENSO conditions. *J Clim* 25:5374–5385
- Liebmann B, Smith CA (1996) Description of a complete (interpolated) outgoing longwave radiation dataset. *Bull Am Meteorol Soc* 77:1275–1277
- Lin A, Li T (2008) Energy spectrum characteristics of boreal summer intraseasonal oscillations: climatology and variations during the ENSO developing and decaying phases. *J Clim* 21:6304–6320
- Lin H, Brunet G, Derome J (2008) Forecast skill of the Madden-Julian oscillation in two Canadian atmospheric models. *Mon Weather Rev* 136:4130–4149
- Madden RA, Julian PR (1971) Detection of a 40–50 day oscillation in the zonal wind in the tropical Pacific. *J Atmos Sci* 28:702–708
- Madden RA, Julian PR (1972) Description of global scale circulation cells in the tropics with 40–50 day period. *J Atmos Sci* 29:1109–1123
- Mao JY, Chan JCL (2005) Intraseasonal variability of the South China Sea summer monsoon. *J Clim* 18:2388–2402
- Mullen SL, Schmitz JT, Rennó NO (1998) Intraseasonal variability of the summer monsoon over southeast Arizona. *Mon Weather Rev* 126:3016–3035
- Rashid HA, Hendon HH, Wheeler MC, Alves O (2011) Prediction of the Madden-Julian oscillation with the POAMA dynamical prediction system. *Clim Dyn* 36:649–661
- Saha S et al (2006) The NCEP climate forecast system. *J Clim* 19:3483–3517
- Saha S et al (2010) The NCEP Climate Forecast System reanalysis. *Bull Am Meteorol Soc* 91:1015–1057
- Saha S et al (2013) The NCEP Climate Forecast System version 2. *J Clim* (submitted)
- Seo KH (2009) Statistical-dynamical prediction of the Madden-Julian oscillation using NCEP Climate Forecast System (CFS). *Int J Climatol*. doi:10.1002/joc.1845
- Vitart F, Woolnough S, Balmaseda MA, Tompkins AM (2007) Monthly forecast of the Madden-Julian oscillation using a coupled GCM. *Mon Weather Rev* 135:2700–2715
- Waliser DE, Lau KM, Kim JH (1999) The influence sea surface temperatures on the Madden-Julian oscillation: perturbation experiment. *J Atmos Sci* 56:333–358
- Wang W, Xie P, Yoo SH, Xue Y, Kumar A, Wu X (2010) An assessment of the surface climate in the NCEP climate forecast system reanalysis. *Clim Dyn* 37:1601–1620
- Weare BC, Nasstrom JS (1982) Examples of extended empirical orthogonal function analyses. *Mon Weather Rev* 110:481–485
- Webster PJ (1983) Mechanisms of monsoon low-frequency variability: surface hydrological effects. *J Atmos Sci* 40:2110–2124
- Wen M, Zhang R (2007) Role of the quasi-biweekly oscillation in the onset of convection over the Indochina Peninsula. *Q J R Meteorol Soc* 133:433–444
- Wen M, Yang S, Higgins RW, Zhang R (2011) Characteristics of the dominant modes of atmospheric quasi-biweekly oscillation over tropical–subtropical Americas. *J Clim* 24:3956–3970
- Woolnough SJ, Slingo JM, Hoskins BJ (2000) The relationship between convection and sea surface temperature on intraseasonal timescale. *J Clim* 13:2086–2104
- Wu PL, Li CY (1990) The 10–20 day oscillation in the atmosphere. *Collection of atmospheric science*. Science Press, Beijing, pp 147–159 (in Chinese)
- Wu PL, Luo HB (1987) An energetic study of low frequency oscillation in the tropical troposphere. *J Trop Meteorol* 3(2):105–112 (in Chinese)
- Wu RG, Kirtman BP, Pegion K (2008) Local rainfall-SST relationship on subseasonal time scales in satellite observations and CFS. *Geophys Res Lett* 35:L22706. doi:10.1029/2008GL035883
- Xue Y, Huang B, Hu ZZ, Kumar A, Wen C, Behringer D, Nadiga S (2010) An assessment of oceanic variability in the NCEP climate forecast system reanalysis. *Clim Dyn* 37:2511–2539
- Yang J, Wang B, Wang B, Bao Q (2010) Biweekly and 21–30-day variations of the subtropical summer monsoon rainfall over the lower reach of the Yangtze River Basin. *J Clim* 23:1146–1159
- Yasunari T (1981) Structure of an Indian summer monsoon system with around 40-day period. *J Meteorol Soc Jpn* 59:336–354
- Zhou W, Chan JCL (2005) Intraseasonal oscillations and the South China Sea summer monsoon onset. *Int J Climatol* 25:1585–1609